

SUPER-RESOLUTION OF BVOC EMISSION MAPS VIA DOMAIN ADAPTATION

Antonio Giganti, Sara Mandelli, Paolo Bestagini, Marco Marcon, Stefano Tubaro

Dipartimento di Elettronica, Informazione e Bioingegneria - Politecnico di Milano - Milan, Italy

ABSTRACT

Enhancing the resolution of Biogenic Volatile Organic Compound (BVOC) emission maps is a critical task in remote sensing. Recently, some Super-Resolution (SR) methods based on Deep Learning (DL) have been proposed, leveraging data from numerical simulations for their training process. However, when dealing with data derived from satellite observations, the reconstruction is particularly challenging due to the scarcity of measurements to train SR algorithms with. In our work, we aim at super-resolving low resolution emission maps derived from satellite observations by leveraging the information of emission maps obtained through numerical simulations. To do this, we combine a SR method based on DL with Domain Adaptation (DA) techniques, harmonizing the different aggregation strategies and spatial information used in simulated and observed domains to ensure compatibility. We investigate the effectiveness of DA strategies at different stages by systematically varying the number of simulated and observed emissions used, exploring the implications of data scarcity on the adaptation strategies. To the best of our knowledge, there are no prior investigations of DA in satellite-derived BVOC maps enhancement. Our work represents a first step toward the development of robust strategies for the reconstruction of observed BVOC emissions.

Index Terms— Biogenic Emission, BVOC, Isoprene, Image Super-Resolution, Domain Adaptation

1. INTRODUCTION

Biogenic Volatile Organic Compounds (BVOCs) have been largely studied in the last two decades [1]–[4] as they play critical roles in atmospheric chemistry [5], [6], promoting the formation of low-level ozone and secondary organic aerosols that strongly impact air quality and the planet’s radiative budget [7]. Studying BVOC emissions proves paramount for numerical evaluations of past, current, and future air quality and climate conditions [6]. To perform these BVOC-based studies on climate, quantitative estimations of BVOC emissions are required for numerical evaluations.

However, BVOC measurements are often limited in space and time, and acquiring fine-grained BVOC emission maps over a large region is costly and time-consuming [4], [8]. Therefore, the available BVOC emission maps might be not enough for reliable simulations of atmospheric, climate, and forecasting models [9]. To solve this issue, image Super-Resolution (SR) techniques can be applied to BVOC acquisitions, in order to generate a denser spatial grid of emission maps by starting from a coarser one [10].

Recently, some methods have been proposed to super resolve BVOC emission by leveraging Deep Learning (DL) models [10], [11]. Despite their promising performance, the main limitation of the currently available approaches is that they require to be trained

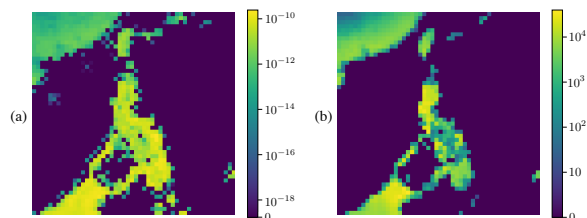


Fig. 1: Comparison between BVOC emission maps corresponding to the same geographical area but to different domains: (a) simulated data (b) observed data. Emission values and patterns differ according to the data aggregation strategies adopted [12], [14].

and tested on datasets with similar characteristics, otherwise there is strong risk of encountering data domain mismatch, resulting in unreliable BVOC reconstructions [10].

For instance, in many realistic scenarios, there might be the need to super-resolve BVOC maps derived from actual satellite measurements, at the same time disposing of few data of this kind at training stage, due to the difficulty in acquiring these emissions. A possible solution could be to train the SR models on numerically simulated BVOC emission data and use them to super resolve the real measurements. However, the two data domains might report different characteristics in terms of dynamic range and temporal aggregation.

Numerically simulated data are typically aggregated over brief periods to capture short-term variability, smoothing out the long-term characteristics [9], [12]. Contrarily, satellite observations are typically aggregated over long time ranges to reduce the effects of random errors in the measurements and increase the signal-to-noise ratio [13]–[15]. In addition, climate satellite data often comes from non-geostationary satellites, binding the temporal resolution of measurements to the satellite’s revisit time. Moreover, weather conditions may be an obstacle to measurements in specific geographic areas, hindering the possibility to acquire information in a short-term interval. All these peculiar characteristics inevitably lead to a domain-shift between simulated and observed data. For example, Fig. 1 depicts two BVOC emission maps related to the same geographical area but to different data domains, i.e., simulated or observed. It is noticeable a smoother behaviour of observed data with respect to simulated ones which present more high spatial frequency content. Notice also the differences in the dynamic ranges.

For these reasons, we propose to investigate the capabilities of existing SR algorithms to super resolve emission maps derived from satellite observations. We train the DL models by leveraging numerically simulated data. To counteract the potential domains mismatch, we investigate the use of Domain Adaptation (DA) [16] strategies, with the scope of mitigating the problems that arise in dealing with data coming from a domain other than the one used in training.

Several approaches have been proposed to solve the adaptation to different domains [17]–[19]. However, to the best of our knowledge, no prior studies tackled DA for BVOC emission. We consider the realistic condition of scarcity of observed data, pushing DA to the limits in case an extremely reduced set of satellite observations can be used to perform the DA.

This work was supported by the Italian Ministry of University and Research (MUR) and the European Union (EU) under the PON/REACT project.

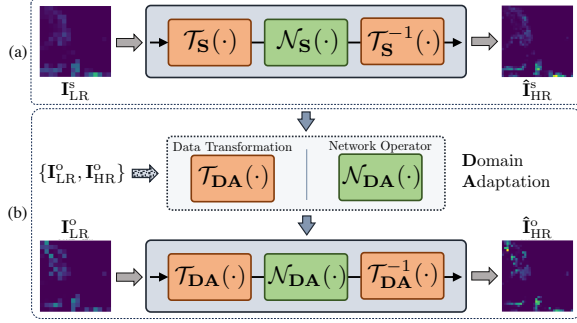


Fig. 2: (a) The proposed Super-Resolution (SR) system [10], which proved valid for dealing with BVOC emission maps of **S** domain; (b) The proposed DA strategies: *Data Transformation* adaptation - $\mathcal{T}_{\text{DA}}(\cdot)$ and *Network Operator* adaptation - $\mathcal{N}_{\text{DA}}(\cdot)$, that take into account the existing domain-shift between emission maps of the **S** and **O** domains.

2. DOMAIN ADAPTATION FOR SATELLITE-DERIVED BVOC ENHANCEMENT

Our goal is to super-resolve Low Resolution (LR) BVOC emission maps derived from satellite observations. We do so by exploiting the knowledge of emission maps obtained from numerical simulations. We denote with **S** the *S(imulated)* and with **O** the *O(bserve)* data domain. The former is obtained through numerical simulations, while the latter is derived from actual satellite observations.

In our previous work [10], we tackled the problem of recovering High Resolution (HR) emission maps starting from LR versions, considering only *numerically simulated* data. We estimated HR simulated emissions $\hat{\mathbf{I}}_{\text{HR}}^{\text{s}}$ by starting from LR emissions $\mathbf{I}_{\text{LR}}^{\text{s}}$ as (see Fig.2(a)):

$$\hat{\mathbf{I}}_{\text{HR}}^{\text{s}} = \mathcal{T}_{\text{S}}^{-1}(\mathcal{N}_{\text{S}}(\mathcal{T}_{\text{S}}(\mathbf{I}_{\text{LR}}^{\text{s}}))), \quad (1)$$

being \mathcal{T}_{S} a data transformation applied to LR simulated emissions [20], [21], \mathcal{N}_{S} a Neural Network (NN) operator [22] and $\mathcal{T}_{\text{S}}^{-1}$ the inverse transformation of \mathcal{T}_{S} . Both \mathcal{T}_{S} and \mathcal{N}_{S} operators were learnt from a training set of *simulated* emissions, meaning they were tailored to the domain of data under investigation, i.e., the domain **S**.

In this work, we propose to super-resolve emission maps derived from satellite *observations* (domain **O**) by leveraging data obtained through numerical *simulations* (domain **S**). To make the most out of the information derived from simulations, an adaptation between the two domains becomes necessary, as we show in our experimental analysis (Sec. 4). Fig. 2(b) shows a simplified scheme of our method. We propose two different Domain Adaptation (DA) strategies: (i) data transformation adaptation; (ii) network operator adaptation.

Data Transformation Adaptation. In the first scenario, we estimate a non-parametric data transformation \mathcal{T}_{DA} from a pool of emissions from domain **O** to adapt the different aggregation strategies and dynamic ranges of both domains and, at the same time, consider the lack of data from the **O** domain compared to the **S**. To highlight the potential advantages of our proposal, we do not modify the NN operator, exploiting the same \mathcal{N}_{S} as in (1), i.e., the NN trained on simulated data. HR observed emissions $\hat{\mathbf{I}}_{\text{HR}}^{\text{o}}$ can be estimated as

$$\hat{\mathbf{I}}_{\text{HR}}^{\text{o}} = \mathcal{T}_{\text{DA}}^{-1}(\mathcal{N}_{\text{S}}(\mathcal{T}_{\text{DA}}(\mathbf{I}_{\text{LR}}^{\text{o}}))). \quad (2)$$

Network Operator Adaptation. In the second scenario, we extend the DA to the NN operator as well. In detail, we investigate the influence of fine-tuning the NN pre-trained on simulated data by injecting some knowledge of the target domain **O**. We estimate HR observed emissions $\hat{\mathbf{I}}_{\text{HR}}^{\text{o}}$ as

$$\hat{\mathbf{I}}_{\text{HR}}^{\text{o}} = \mathcal{T}_{\text{DA}}^{-1}(\mathcal{N}_{\text{DA}}(\mathcal{T}_{\text{DA}}(\mathbf{I}_{\text{LR}}^{\text{o}}))). \quad (3)$$

In Sec. 4, we provide more details on the pursued experimental campaign, analyzing the two proposed DA strategies.

3. DATASET

To validate our approach, we use different datasets belonging to the **S(imulated)** and the **O(bserve)** domains.

S(imulated) Domain. We use the most recent high-resolution global coverage biogenic emission inventory presented in [12]. This can be considered a bottom-up approach since these data are obtained through a simulation of the Model of Emissions of Gases and Aerosols from Nature (MEGAN) [6], a well-known semi-empirical modeling framework embedded into several Earth system and chemical transport models [5]. The inventory includes emissions from BVOCs covering the entire Earth surface in the period of 2000-2019, with a 0.25° spatial resolution. Emissions are reported as hour profiles and are averaged monthly. We refer to this dataset as \mathcal{D}_{S} since it is obtained from numerical simulations.

O(bserve) Domain. We investigate the emission maps derived from two satellite instruments: (i) the Global Ozone Monitoring Experiment-2 (GOME-2) on the EUMETSAT-Metop-A satellite, for the period 2007-2012 [14]; (ii) the Ozone Monitoring Instrument (OMI) on the NASA-Aura (EOS/Chem-1) satellite, for the period 2005-2014 [15]. Both the top-down datasets are available on 0.50° spatial resolution. Emissions are reported as daily averaged profiles. To make a meaningful performance comparison between the two datasets, we consider emissions from the same acquisition years, thus the ones from 2007 to 2012. We refer to the datasets from the GOME-2 and the OMI instruments as \mathcal{D}_{O_1} and \mathcal{D}_{O_2} , respectively.

Experimental dataset. From all the considered datasets, we select only isoprene emission maps, being it the most contributing BVOC in terms of global emission and atmospheric impact [3], [12].

Emission maps of \mathcal{D}_{O_1} and \mathcal{D}_{O_2} datasets present a grid of 720×360 cells. The emission maps of \mathcal{D}_{S} instead cover the same geographical areas of the observed data but comprise 1440×720 cells, since the spatial resolution is twice. For our experiments, we computed also a version of \mathcal{D}_{S} with a spatial resolution of 0.50° , in order to match the resolution of the observed data.

We also work with a subset of \mathcal{D}_{S} , considering emission maps of the same acquisition years of \mathcal{D}_{O} datasets, thus 2007-2012. This enables to perform more realistic comparisons with satellite-derived data. We refer to this subset as \mathcal{D}_{S_T} since it is limited in *Time*.

For each dataset, we slice the emission maps to obtain smaller non-overlapped patches of 32×32 cells, following the steps presented in our previous work [10]. These can be considered our ground truth HR emission maps \mathbf{I}_{HR} . The total number of HR emission patches in \mathcal{D}_{S} is almost 630K at 0.25° and 73K at 0.50° ; \mathcal{D}_{S_T} includes around 187K HR patches at 0.25° and 22K at 0.50° ; each \mathcal{D}_{O} datasets contains almost 16K emission patches at 0.50° .

We generate LR patches by performing bicubic downsampling, obtaining emission maps \mathbf{I}_{LR} of 16×16 cells. Our goal is estimating HR patches from LR ones, with an upscale factor equal to 2.

4. EXPERIMENTAL RESULTS

Experimental Setup. When working with dataset \mathcal{D}_{S} , we train the network \mathcal{N}_{S} by adopting a 70/20/10% splitting strategy for train/validation/test. For the remaining datasets (\mathcal{D}_{S_T} , \mathcal{D}_{O_1} and \mathcal{D}_{O_2}), we split the emission patches considering 2007-2010 for training, 2011 for validation, and 2012 for testing. We always keep an equal amount of patches in all the tests, limiting this according to the dataset with the lowest cardinality, so the \mathcal{D}_{O} datasets.

Table 1: Results in perfect knowledge scenario (no DA required). Training times are reported as a fraction of the time spent for the case $\mathcal{D}_S, 0.50^\circ \rightarrow 0.25^\circ$ (first row).

Dataset	Spatial Resolution	No.Patches	NMSE [dB]	SSIM	Training Time [%]
\mathcal{D}_S	$0.50^\circ \rightarrow 0.25^\circ$	630192	-23.83	0.988	100 [ref]
	$1.00^\circ \rightarrow 0.50^\circ$	73152	-19.40	0.988	17.60
\mathcal{D}_{S_T}	$0.50^\circ \rightarrow 0.25^\circ$	187488	-26.54	0.989	23.15
	$1.00^\circ \rightarrow 0.50^\circ$	21864	-22.33	0.989	10.32
\mathcal{D}_{O_1}	$1.00^\circ \rightarrow 0.50^\circ$	16495	-15.68	0.979	3.73
\mathcal{D}_{O_2}	$1.00^\circ \rightarrow 0.50^\circ$	16495	-18.07	0.977	3.73

We evaluate the SR performances in terms of Structural Similarity Index Measure (SSIM) and Normalized Mean Squared Error (NMSE), defined as the Mean Squared Error (MSE) between \mathbf{I}_{HR} and $\hat{\mathbf{I}}_{HR}$, normalized by the average of \mathbf{I}_{HR}^2 . A good result is the one with high SSIM and/or low NMSE.

We implement and train our method using an NVIDIA Tesla V100 PCIe 16 GB GPU, running on an Intel Xeon Gold 6246 CPU.

Perfect Knowledge Scenario. In this scenario, we investigate the performance in case a subset of HR data of the same domain of the testing ones is available for training, i.e., no DA is needed. We use these results to show the effectiveness of the proposed SR method on the different data domains under investigation.

To this purpose, we apply (1) to the various datasets we experiment on, training a NN operator \mathcal{N} and estimating the data transformation \mathcal{T} from the specific training set involved. For instance, when working with \mathcal{D}_{O_1} , we exploit its HR training set to estimate specific \mathcal{T}_{O_1} and \mathcal{N}_{O_1} operators by following our past methodology [10]. Results achieved across the different datasets are shown in Tab. 1. For clarity’s sake, Tab. 1 includes additional information: for each dataset, we report the total number of patches in the set and the time required for training the SR system.

For \mathbf{S} datasets, i.e., \mathcal{D}_S and \mathcal{D}_{S_T} , the higher the spatial resolution, the better the performance. We believe this depends on the emissions’ spatial resolution which impacts their high-frequency information. Indeed, patches at 0.50° inherently contain more spatial information than those at 1.00° . This results in a more spatially detailed emission map.

We can notice a significant reconstruction improvement when considering \mathcal{D}_{S_T} with respect to \mathcal{D}_S . Indeed, as we have shown in our previous work [10], the splitting strategy of \mathcal{D}_{S_T} improves the performance since the system can capture these temporal dynamics of the emission and generalize its predictions to unseen years, reflecting real-world applications.

When changing the data domain, results report a performance drop. Focusing on the case $1.00^\circ \rightarrow 0.50^\circ$ spatial resolution, results on \mathbf{O} datasets are at least 4 dB worse than the best results of \mathbf{S} datasets. We believe the emissions belonging to the \mathbf{S} domain inherently contain less noise than those of \mathbf{O} since they are numerically simulated and, therefore, easier to describe and reconstruct.

We also evaluate the impact of the computational time required for training on the different datasets. On \mathbf{S} domain, training on time-limited data, i.e., \mathcal{D}_{S_T} , not only leads to superior performance but also strongly reduces the computation time since a smaller number of patches is considered for training. On \mathbf{O} domain, the training time is extremely reduced, due to the low cardinality of the datasets.

Zero Knowledge Scenario. This scenario assumes we do not have any HR observed data at disposal. Hence, we estimate HR emission maps of \mathbf{O} domain by leveraging only the operators learnt from simulated data (\mathbf{S} domain).

Our experimental analysis shows that training either on \mathcal{D}_S or \mathcal{D}_{S_T} and testing on \mathcal{D}_O datasets results in drastic performance drops. Indeed, the NMSE is fixed at 0 dB for both \mathcal{D}_{O_1} and \mathcal{D}_{O_2} .

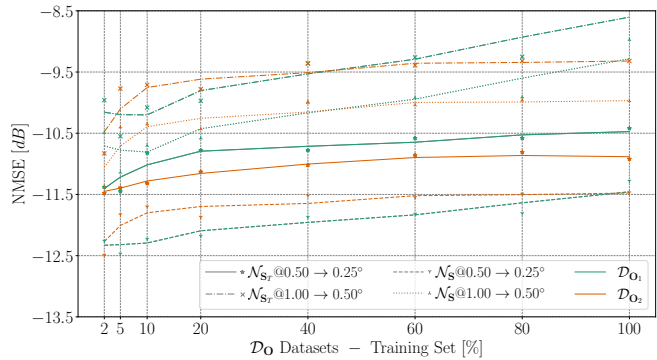


Fig. 3: Average NMSE achieved by varying the amount of patches of the \mathbf{O} domain used to train the \mathcal{T}_{DA} emission transformation. The point values represent the mean value, averaged over three random subsets of the \mathcal{D}_O datasets, for each percentage. Lines report the smoothed trends of these experiment.

We believe the huge differences in data statistics from these two domains strongly impact the reconstruction of the super resolved emissions. This motivates the investigation of DA strategies.

Data Transformation Adaptation. This strategy supposes that a certain portion of observed data is available to the analyst. These data can be exploited to estimate a non-parametric transformation \mathcal{T}_{DA} characterizing the emission statistics of the \mathbf{O} domain. In specific, we investigate how many data from this domain impact the adaptation process, considering an increasing percentage of the \mathcal{D}_{O_1} and \mathcal{D}_{O_2} training partitions for estimating the \mathcal{T}_{DA} transformation.

As reported in Section 2, we keep the NN operator trained on the \mathbf{S} domain and estimate the final super-resolved emissions through (2). We exploit either \mathcal{D}_S or \mathcal{D}_{S_T} datasets for training. Since the \mathbf{S} domain has higher native spatial resolution than the \mathbf{O} , we train on different spatial resolutions, addressing the $0.50^\circ \rightarrow 0.25^\circ$ case and its relative coarser version, from 1.00° to 0.50° . Then, we test on \mathcal{D}_O datasets to pass from 1.00° to 0.50° .

Fig. 3 reports the system performance trend. Training \mathcal{T}_{DA} with a small percentage of emission patches gives a slightly better generalization performance and captures the underlying statistics of the data more accurately. This is a counter-intuitive result since having more data for training a model generally improves its performance on unseen data. However, this effect consistently holds across multiple experiments, indicating the genuine nature of this phenomenon.

Training with higher spatial resolution \mathbf{S} patches, i.e., from 0.50° to 0.25° , leads to a significant improvement in the reconstruction of \mathbf{O} emission profiles. We believe higher spatial resolution in the training phase allows the network to learn high-frequency features that positively impact the reconstruction process.

In addition, notice that exploiting \mathcal{N}_S , which uses emissions from \mathcal{D}_S dataset, has positive impact in reconstructing \mathcal{D}_O emissions compared to \mathcal{N}_{S_T} . This was expected, due to the huge number of patches used in training. Nonetheless, considering also the training timings in Tab. 1, \mathcal{N}_{S_T} results in slightly lower performance than \mathcal{N}_S but leads to a substantial reduction in the computations.

Given these reasons, we select the model trained on the higher spatial resolution ($0.50^\circ \rightarrow 0.25^\circ$) and on \mathcal{D}_{S_T} emissions as a baseline for subsequent DA experiments.

Network Operator Adaptation. In this strategy, we systematically inject a portion of data belonging to \mathcal{D}_O datasets in our system’s learning (training and validation) phase. The remaining part of the dataset used in learning phase comprises emission patches belonging to the \mathbf{S} domain, specifically to the \mathcal{D}_{S_T} dataset. For instance, the 0% injection case corresponds to our preliminary investigations, where we use only data from the \mathbf{S} domain for training the NN opera-

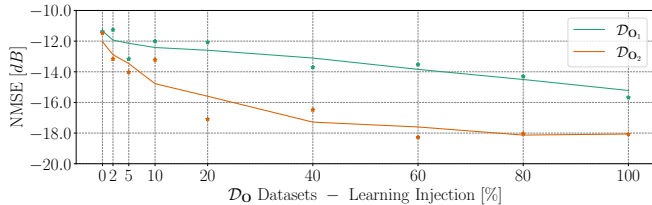


Fig. 4: Average NMSE achieved by the *Network Operator* adaptation strategy, in which we train the NN operator by varying the amount of injected patches from the **O** domain.

tor. Contrarily, the 100% injection case is related to the last two rows of Table 1, which correspond to the perfect knowledge scenario.

The NN operator is not trained from scratch. We fine-tune the NN, adapting the network weights pre-trained on **S** data (\mathcal{D}_{S_T} dataset, from 0.50° to 0.25°) to handle data from the target domain **O**, thus reducing the inherent domain-shift. For this reason, we refer to the new NN operator as \mathcal{N}_{DA} . Regarding the data transformation applied to **O** data, we select the best configuration found for the data transformation adaptation \mathcal{T}_{DA} (see Fig. 3). Final super-resolved emissions from **O** domain are obtained using (3).

Fig.4 reports the performances by varying the number of emission maps from **O** domain used in the injection process. We can notice a relevant trend: increasing the percentage of data injection benefits the SR quality for both the \mathcal{D}_O datasets. For \mathcal{D}_{O_1} emissions, just a 5% injection gives an improvement of 1.8 dB respect to the 0% case. For \mathcal{D}_{O_2} emissions, a suitable trade-off between the amount of data and performance can be found when using 20% injection, with an improvement of 5.6 dB with respect to the 0% case. Above the 60% of data injection, results are comparable with the perfect knowledge scenario. For the sake of clarity, we report at this link¹ some additional results.

5. CONCLUSIONS

In this work, we tackled the problem of Super-Resolution (SR) of BVOC emission maps derived from satellite observations. Existing SR methods are based on Deep Learning (DL) and are effective on numerically simulated emission maps, thanks to the huge amount of data at disposal for training the models. This is not true when dealing with BVOC emission maps of satellite-derived data which are often scarce, thus limiting the SR performance.

To solve this issue, we proposed to exploit the information coming from numerically simulated emission maps. However, some Domain Adaptation (DA) from the simulated to the observed data domain is necessary, since the two domains are characterized by extremely different spatial frequency behaviour and dynamic ranges.

Therefore, we proposed two DA strategies to solve the SR of BVOC emission maps of satellite-derived data. First, we investigated a data transformation adaptation to adapt the different aggregation strategies and dynamics of simulated and observed data domains. Then, we explored a neural network adaptation, analyzing the influence of fine-tuning DL-based models on real observations. Our experimental results shows that DA strategies are the key for achieving high quality reconstruction on emission maps derived from satellite observations, even in data scarcity conditions.

6. REFERENCES

- [1] P. Ciccioli, C. Silibello, S. Finardi, *et al.*, “The potential impact of biogenic volatile organic compounds (bvocs) from terrestrial vegetation on a mediterranean area using two different emission models,” *Agricultural and Forest Meteorology*, vol. 328, p. 109 255, 2023.

- [2] A. Tani and T. Mochizuki, “Review: Exchanges of volatile organic compounds between terrestrial ecosystems and the atmosphere,” *Journal of Agricultural Meteorology*, vol. 77, pp. 66–80, 2021.
- [3] B. Opacka, J.-F. Müller, T. Stavrou, *et al.*, “Global and regional impacts of land cover changes on isoprene emissions derived from spaceborne data and the megan model,” *Atmospheric Chemistry and Physics*, vol. 21, no. 11, pp. 8413–8436, 2021.
- [4] D. Fu, D. B. Millet, K. C. Wells, *et al.*, “Direct retrieval of isoprene from satellite-based infrared measurements,” *Nature Communications*, vol. 10, p. 3811, 2019.
- [5] M. Cai, C. An, and C. Guy, “A scientometric analysis and review of biogenic volatile organic compound emissions: Research hotspots, new frontiers, and environmental implications,” *Renewable and Sustainable Energy Reviews*, vol. 149, pp. 1–15, 2021.
- [6] A. B. Guenther, X. Jiang, C. L. Heald, *et al.*, “The Model of Emissions of Gases and Aerosols from Nature version 2.1 (MEGAN2.1): An extended and updated framework for modeling biogenic emissions,” *Geoscientific Model Development*, vol. 5, pp. 1471–1492, 2012.
- [7] C. Calafapietra, S. Fares, F. Manes, *et al.*, “Role of Biogenic Volatile Organic Compounds (BVOC) emitted by urban trees on ozone concentration in cities: A review,” *Environmental Pollution*, vol. 183, pp. 71–80, 2013.
- [8] C. N. Hewitt, B. Langford, M. Possell, *et al.*, “Quantification of VOC emission rates from the biosphere,” *TrAC Trends in Analytical Chemistry*, vol. 30, pp. 937–944, 2011.
- [9] M. Bauwens, T. Stavrou, J.-F. Müller, *et al.*, “Recent past (1979–2014) and future (2070–2099) isoprene fluxes over europe simulated with the megan–mohycan model,” *Biogeosciences*, vol. 15, no. 12, pp. 3673–3690, 2018.
- [10] A. Giganti, S. Mandelli, P. Bestagini, *et al.*, “Super-resolution of bvoc maps by adapting deep learning methods,” *arXiv preprint arXiv:2302.07570v2*, 2023.
- [11] A. Giganti, S. Mandelli, P. Bestagini, *et al.*, “Multi-bvoc super-resolution exploiting compounds inter-connection,” *arXiv preprint arXiv:2305.14180v1*, 2023.
- [12] K. Sindelarova, J. Markova, D. Simpson, *et al.*, “High-resolution biogenic global emission inventory for the time period 2000–2019 for air quality modelling,” *Earth System Science Data*, vol. 14, pp. 251–270, 2022.
- [13] H. Wang, Q. Wu, A. B. Guenther, *et al.*, “A long-term estimation of biogenic volatile organic compound (bvoc) emission in china from 2001–2016: The roles of land cover change and climate variability,” *Atmospheric Chemistry and Physics*, vol. 21, no. 6, pp. 4825–4848, 2021.
- [14] I. De Smedt, M. Van Roozendaal, T. Stavrou, *et al.*, “Improved retrieval of global tropospheric formaldehyde columns from gome-2/metop-a addressing noise reduction and instrumental degradation issues,” *Atmospheric Measurement Techniques*, vol. 5, no. 11, pp. 2933–2949, 2012.
- [15] M. Bauwens, T. Stavrou, J.-F. Müller, *et al.*, “Nine years of global hydrocarbon emissions based on source inversion of omi formaldehyde observations,” *Atmospheric Chemistry and Physics*, vol. 16, no. 15, pp. 10 133–10 158, 2016.
- [16] S. Ben-David, J. Blitzer, K. Crammer, *et al.*, “A theory of learning from different domains,” en, *Machine Learning*, vol. 79, no. 1, pp. 151–175, 2010.
- [17] N. Yadav, “DeepAQ: Unsupervised Domain Adaptation for Air-Quality Mapping Using High-Resolution Satellite Imagery,” en, Open Science Framework, preprint, Jan. 2023.
- [18] M. Xu, M. Wu, K. Chen, *et al.*, “The eyes of the gods: A survey of unsupervised domain adaptation methods based on remote sensing data,” *Remote Sensing*, vol. 14, no. 17, 2022.
- [19] J. Peng, Y. Huang, W. Sun, *et al.*, “Domain adaptation in remote sensing image classification: A survey,” *IEEE Journal of Selected Topics in Applied Earth Observations and Remote Sensing*, vol. 15, pp. 9842–9859, 2022.
- [20] F. Pedregosa, G. Varoquaux, A. Gramfort, *et al.*, “Scikit-learn: Machine learning in Python,” *Journal of Machine Learning Research*, vol. 12, pp. 2825–2830, 2011.
- [21] R. A. Peterson and J. E. Cavanaugh, “Ordered quantile normalization: A semiparametric transformation built for the cross-validation era,” *Journal of Applied Statistics*, vol. 47, no. 13-15, pp. 2312–2327, 2020.
- [22] T. Dai, J. Cai, Y. Zhang, *et al.*, “Second-Order Attention Network for Single Image Super-Resolution,” in *IEEE Conference on Computer Vision and Pattern Recognition (CVPR)*, 2019.

¹<https://github.com/polimi-ispl/sr-bvoc>